AGU ADVANCING EARTH AND SPACE SCIENCES

AGU Advances

RESEARCH ARTICLE
10.1029/2024AV001508

Megapluvials in Southwestern North America

Benjamin I. Cook[1,2], **A. Park Williams**[3,4], **Jason E. Smerdon**[2,5], **Kate Marvel**[1], and **Richard Seager**[2]

[1]NASA Goddard Institute for Space Studies, New York, NY, USA, [2]Ocean & Climate Physics, Lamont-Doherty Earth Observatory, New York, NY, USA, [3]Department of Geography, University of California-Los Angeles, Los Angeles, CA, USA, [4]Tree Ring Lab, Lamont-Doherty Earth Observatory, New York, NY, USA, [5]The Climate School, Columbia University, New York, NY, USA

Peer Review The peer review history for this article is available as a PDF in the Supporting Information.

Key Points:

- Pluvials in Southwestern North America occur as often as droughts, including two 20th century megapluvials from 1905 to 1923 and 1978-1999
- The 1978–1999 megapluvial was the wettest interval of the last 1200 years, even more extreme than the early 21st century megadrought
- The extreme wetness of 1978–1999 was forced by anomalously warm and persistent Pacific SSTs

Supporting Information:

Supporting Information may be found in the online version of this article.

Correspondence to:

B. I. Cook,
benjamin.i.cook@nasa.gov

Citation:

Cook, B. I., Williams, A. P., Smerdon, J. E., Marvel, K., & Seager, R. (2025). Megapluvials in Southwestern North America. *AGU Advances*, *6*, e2024AV001508. https://doi.org/10.1029/2024AV001508

Received 23 SEP 2024
Accepted 10 FEB 2025

Author Contributions:

Conceptualization: Benjamin I. Cook, A. Park Williams, Jason E. Smerdon, Kate Marvel, Richard Seager
Data curation: Benjamin I. Cook
Formal analysis: Benjamin I. Cook, A. Park Williams, Jason E. Smerdon, Kate Marvel, Richard Seager

Abstract Droughts over the last century in Southwestern North America (SWNA) have had severe consequences for people and ecosystems across the region, most recently during the early 21st-century megadrought (2000–2022). The 20th century, however, was bracketed by two extended pluvials that also had significant impacts in the region. We use a 1,224 years (800–2023 CE) record of observed and reconstructed soil moisture, in concert with a paleoclimate reanalysis product, to place the 20th-century pluvials in a longer-term context and investigate the occurrence and dynamics of similar events in the Common Era. Analyses of the soil moisture reconstruction demonstrate that pluvials and megapluvials are as ubiquitous as droughts and megadroughts over the last millennium. The early (19 years; 1905–1923) and late (22 years; 1978–1999) 20th-century pluvials rank as the second and first wettest in the record, respectively, positioning these as events on par with the most extreme megadroughts. Pluvials show a strong association with tropical Pacific (warm) sea surface temperatures (SSTs) during the 20th century and over the prior millennium, though the role of the tropical Atlantic is much more uncertain and ambiguous. Using a Bayesian hierarchical modeling approach trained on the pre-industrial period (800–1849 CE), we find that the record setting late 20th-century megapluvial likely occurred as a consequence of anomalously strong Pacific sea surface temperature forcing. This work establishes pluvial and megapluvial events as intrinsic components of Common Era hydroclimate variability in SWNA, comparable in importance to droughts and megadroughts.

Plain Language Summary We use a record of soil moisture that extends over one thousand years to investigate the occurrence and causes of modern and historical pluvial events. We find that pluvials and megapluvials (i.e., extreme and prolonged wet periods) are just as common as droughts and megadroughts over the last thousand years. Notably, these megapluvials include two major events that occurred near the beginning (1905–1923) and end (1978–1999) of the 20th century, which we show were the two wettest periods of the last millennium. Much like droughts, pluvials are promoted by changes in ocean temperatures in the tropical Pacific and Atlantic, and we find that the record-setting 1978–1999 megapluvial was likely due to anomalously persistent warm conditions in the Pacific.

1. Introduction

Two extended pluvial events marked the beginning and end of the 20th century in western North America, affecting ecosystems, water resources, and economic development across the region. The first, in the early 1900s, was one of the wettest periods in the Colorado River Basin of the last millennium (Fye et al., 2003; Meko et al., 2022; Stockton & Jacoby, 1976; Woodhouse et al., 2005, 2006), boosting the average flow in the Colorado River to 16.4 million-acre-feet per year (Fall & Davis, 2022). While other estimates showed substantially lower long-term average discharge (La Rue et al., 1925), the high levels during this period would serve as the basis for the overly generous water allocations underpinning the Colorado River Compact of 1922 (Christensen et al., 2004), setting the stage for major conflicts across stakeholders in the region (Fleck & Castle, 2022; Ge et al., 2023; Kuhn & Fleck, 2019). The late 20th century was another extremely wet period in the western United States that coincided with rapid economic and population growth in the region (Rasker, 2016). This was an interval of reduced fire activity (Dennison et al., 2014; Juang et al., 2022), a substantially enhanced terrestrial carbon sink (Nemani et al., 2002), and record or near record levels in the two most important water reservoirs in the region, Lakes Mead and Powell (Forsythe et al., 2012; Holdren & Turner, 2010). Notably, the extreme wetness during this pluvial stands in sharp contrast with the 21st-century megadrought that followed (Williams et al., 2020, 2022), a wet-to-dry transition that was one of the fastest multi-decadal drying trends of the last

Funding acquisition: Benjamin I. Cook, A. Park Williams, Jason E. Smerdon, Kate Marvel, Richard Seager
Investigation: Benjamin I. Cook
Methodology: Benjamin I. Cook, A. Park Williams, Jason E. Smerdon, Kate Marvel, Richard Seager
Project administration: Benjamin I. Cook
Resources: Benjamin I. Cook
Software: Benjamin I. Cook, A. Park Williams, Jason E. Smerdon, Kate Marvel, Richard Seager
Supervision: Benjamin I. Cook
Validation: Benjamin I. Cook, A. Park Williams, Jason E. Smerdon, Kate Marvel, Richard Seager
Visualization: Benjamin I. Cook, Kate Marvel
Writing – original draft: Benjamin I. Cook, A. Park Williams, Jason E. Smerdon, Kate Marvel, Richard Seager
Writing – review & editing: Benjamin I. Cook, A. Park Williams, Jason E. Smerdon, Kate Marvel, Richard Seager

millennium (Bishop et al., 2021; B. I. Cook et al., 2021). Pluvials have therefore arguably had as much of an impact on people and ecosystems in the West as the major droughts of the 20th century (B. I. Cook et al., 2009; S. D. Schubert et al., 2004; Seager et al., 2005).

Despite their importance, a comprehensive analysis of multi-year pluvials has been lacking to date, highlighting uncertainties in our understanding of the variability, dynamics, and drivers of these events. Specific pluvials in the instrumental and paleoclimate records have been the subject of various studies. These include analyses of events in the mid-1600s (Fye et al., 2003), the early 17th century (Fye et al., 2003; Robeson et al., 2020), the early 1800s (van der Schrier & Barkmeijer, 2007), and the early (Robeson et al., 2020; Stockton & Jacoby, 1976; Woodhouse et al., 2005, 2006) and late (Allen et al., 2013) 20th century. However, it is unclear if multi-year pluvials over the last millennium have similar characteristics to droughts (e.g., frequency, duration, etc.) and if pluvial events analogous to the megadroughts of the Medieval-era (Coats et al., 2016; Herweijer et al., 2007; Steiger et al., 2019) have also occurred. We suggested previously (B. I. Cook et al., 2022) that *megadroughts* could be broadly defined as *"persistent, multi-year drought events that are exceptional in terms of severity, duration, or spatial extent when compared to other regional droughts during the instrumental period or the Common Era"*. To our knowledge, however, similar criteria have not been applied to wet periods to identify *megapluvials* or used to evaluate whether the ostensibly extreme 20th-century pluvials would qualify.

While tropical sea surface temperature (SST) variability is well established as a major driver of drought in western North America (Seager et al., 2005), the role of these same ocean dynamics for pluvials is less understood. Climate model simulations forced by SSTs have definitively demonstrated the important role of cold tropical Pacific forcing for the Medieval megadroughts (Coats et al., 2016; Herweijer et al., 2007; Steiger et al., 2019) and all three decadal-scale instrumental-era droughts: the Dust Bowl of the 1930s (S. D. Schubert et al., 2004), the 1950s drought (Seager et al., 2005), and the early 21st century megadrought (Seager et al., 2023). Warm tropical Atlantic SSTs have also been linked to historical and Medieval-era drought events in the region (McCabe et al., 2004; Nigam et al., 2011; Steiger et al., 2019). Similar analyses for pluvials, however, are much more limited. Climate model simulations forced by observed SST patterns strongly suggest that warm tropical Pacific SSTs were a dominant driver of the late 20th-century pluvial (H.-P. Huang et al., 2005; Seager et al., 2023). Other experiments using early 20th-century SST states, however, have found only a weak or ambiguous role for ocean forcing during the early 20th-century pluvial (B. I. Cook et al., 2011; Seager et al., 2005). A broader analysis is therefore needed to better evaluate the association between tropical SST forcing and extended pluvials.

In the paleoclimate record, analyses are hampered by the paucity of independent ocean temperature reconstructions. This constraint can be remedied by using paleoclimate reanalyses. In this study, we use an updated version of a tree-ring based, millennial-length (800–2023 CE), soil moisture reconstruction from Southwestern North America (SWNA) (Williams et al., 2020, 2022) with a global paleoclimate reanalysis product (Steiger et al., 2018) to investigate the variability and dynamics of extended pluvials and megapluvials in the region. We investigate the major pluvial events of the 20th century, compare their duration and severity to droughts and pluvials over the last millennium, and investigate the most likely climatic drivers. Specifically, we focus on the following research questions: (a) How do pluvials in the paleoclimate record compare to droughts in terms of their frequency, severity, and persistence, and would recent events qualify as megapluvials? (b) How do the climatic drivers (precipitation seasonality, ocean forcing) of the two 20th-century events compare to each other, the early 21st-century megadrought, and past pluvial events? (c) How well can the 20th-century pluvials be explained by tropical SST variability?

2. Materials and Methods

2.1. Observational Data

Precipitation data are from the NOAA Monthly U.S. Climate Gridded Data set (NClimGrid) (Vose et al., 2014), covering the period 1901–2023. This is the same monthly precipitation data set used by Williams et al. (2022) to construct the observation-based soil moisture estimates that served as the target of their soil moisture reconstruction. We also analyze atmospheric circulation during the pluvial events using 200 hPa geopotential heights from version 3 of the 20th Century Reanalyis (1836–2015) (Slivinski et al., 2021). Finally, we use monthly indices of several SST-based climate modes (units K; common interval 1871–2023) known to have strong teleconnections with hydroclimate in western North America. These include the Niño 3.4 index from the HadISST data set (Rayner et al., 2003), Atlantic Multidecadal Oscillation (AMO) index calculated from HadSST version

4.0 (Kennedy et al., 2019), and Pacific Decadal Oscillation (PDO) index calculated from NOAA ERSST version 5 (B. Huang et al., 2017). All three SST indices were recentered to have a mean of zero over their common interval. Note that, while both the PDO and AMO do have extra-tropical expressions in their SST fields, the ultimate forcing of North American hydroclimate originates from the tropical SST component of these modes (Seager & Ting, 2017). Hereinafter, we refer to "tropical SST" forcing by these modes of variability. For all data sets, we calculate 3-month seasonal averages: winter (December–January–February; DJF), spring (March–April–May; MAM), summer (June–July–August; JJA), and fall (September–October–November; SON).

2.2. Soil Moisture Reconstruction

We chose summer soil moisture as our focus for defining pluvials for several reasons. First, there is a long legacy of using summer soil moisture to analyze hydroclimate dynamics and variability in Southwestern North America. This includes analyses using observations (Seager et al., 2023), paleoclimate reconstructions (E. R. Cook et al., 2010), and model simulations of the past and future (B. I. Cook et al., 2021; Herweijer et al., 2006). Second, using soil moisture allows us to leverage two complementary data sets that provide similar soil moisture information: an empirical tree-ring reconstruction and a paleoclimate reanalysis. Using both allows us to assess the robustness of our results and use additional information on ocean forcing provided by the reanalysis. Finally, soil moisture is an integrative metric, sensitive to large-scale antecedent shifts in the surface moisture balance. The summer soil moisture reconstruction that is the focus of our analysis can therefore provide information on hydroclimate across seasons, including the critical cold season dynamics that drive growing season moisture variability in SWNA (see below).

For our analyses, we primarily use the latest, updated version of the tree-ring based reconstruction of 0–200 cm JJA soil moisture anomalies for SWNA developed by Williams et al. (2020, 2022), hereafter referred to as SM-REC. This reconstruction combines empirically constrained soil moisture estimates for the 20th century and later (using inputs from precipitation and evapotranspiration losses calculated from meteorological inputs of temperature, humidity, radiation, and wind speed) with tree-ring reconstructed soil moisture for prior centuries. The reconstruction methodology is based on an ensemble approach to determine the best performing reconstruction at each grid point using different combinations of calibration periods, search radii, and spatial smoothing during the full overlapping period of the tree-ring and instrumental data (1901–1983) (see Methods in Williams et al. (2020)). The tree-ring reconstruction for soil moisture is highly skillful across SWNA, with an average cross-validation $R^2 > 0.80$ after 1400 C.E. and $R^2 > 0.70$ from 800 to 1299 C.E. Our analyses use the reconstruction averaged over the SWNA region (125–105°W, 30–45°N), with tree-ring estimated soil moisture from 800 to 1900 C.E. and the observational estimates from 1901 to 2023, yielding a continuous 1,224 years long record of soil moisture. Soil moisture is expressed in units of standard deviation (σ) relative to a zero baseline, and we scaled the time series to have a mean of zero and unit standard deviation over the entire period of record (800–2023 CE). Further details on the reconstruction methodology can be found in Williams et al. (2020, 2022).

A common concern when using tree-ring estimates of soil moisture is their tendency to capture dry extremes with greater fidelity compared to wet extremes. Trees are generally more sensitive to periods of low soil moisture availability, when they will be water stressed, and less sensitive to periods of extreme wetness, when their water needs will be well satisfied (Fritts, 1976; Sun et al., 2017). To assess the degree to which this could be a concern for our analyses, we compared tree-ring (REC) and observation-based (OBS) soil moisture estimates over the full period of overlap between these two records (1901–1983; Figure S1 in Supporting Information S1). The two soil moisture estimates are highly correlated (Pearson's $r = +0.94$; $p \leq 0.0001$) with a strongly linear relationship and little evidence for bias in either the most extreme wet or dry years. This is largely confirmed when comparing the two pluvial events identified during this period across the two soil moisture data sets: 1905–1923 and 1941–1945. For these events, SM-REC slightly overestimates the magnitude (cumulative severity) of the 1905–1923 megapluvial (SM-OBS $= +17.49\sigma$, SM-REC $= +19.96\sigma$) and slightly underestimates the magnitude of the 1941–1945 pluvial (SM-OBS $= +7.70\sigma$, SM-REC $= +5.41\sigma$).

To further explore possible biases, we analyze the residuals from a regression of SM-REC against SM-OBS over their full overlapping period (1901–1983). First, we conduct a Breusch-Pagan test for heteroskedasticity in the residuals. In the case of a systematic bias in the reconstruction towards over- or underestimation of extreme wet or dry years, we would expect the residuals to have unequal variance. From this test, we cannot reject the null hypothesis ($p = 0.86$) of equal variance, and therefore find no evidence that variance in the residuals is unequal

across the full range of values. Second, we compare the central tendency (median) of the residuals for wet years (SM-OBS $\geq +1.0\sigma$, $n = 19$) against all other residuals (SM-OBS $< +1.0\sigma$, $n = 64$) using a two-sample Wilcoxon Rank Sum test. Comparing the two distributions, we find no significant difference ($p = 0.54$) in the median between these two different residual distributions, further pointing to the lack of a systematic bias for wet events in the reconstruction. We find similar insignificant differences when the most extreme (SM-OBS $\geq +2.0\sigma$) wet values are compared ($p = 0.37$). Given these results, our investigation of pluvials using the employed reconstruction appears to be well justified.

In many regions, soil moisture is strongly influenced by precipitation in antecedent seasons, a consequence of the inherent "memory" of the land surface (Rahmati et al., 2024). For example, Seager et al. (2023) showed that the recent history of summer soil moisture in western North America could be reproduced as a response to cool season precipitation anomalies driven by tropical SST anomalies, even in the absence of model fidelity in simulating summer precipitation. Further, cold season precipitation signals have been documented in tree-ring based reconstructions of summer soil moisture across the Northern Hemisphere extra-tropics, including North America (Baek et al., 2017; St. George et al., 2010). To assess the extent to which antecedent precipitation influences our observational and tree-ring reconstructed 200 cm soil moisture, we compare monthly precipitation against soil moisture over the common period in both soil moisture data sets (1901–1983). Winter and spring precipitation have a strong and significant influence on both SM-OBS and SM-REC (Figure S2 in Supporting Information S1). Observation-based soil moisture (SM-OBS) is significantly ($p \leq 0.05$) correlated (Pearson's r) with precipitation from the previous December through June. Results are similar for the reconstruction (SM-REC), with similar correlation magnitudes, except the period of significant correlation extends through July. For both soil moisture indicators, correlations are highest during the winter through early spring (December–April). The soil moisture metric we consider should therefore provide information on the cold season processes and dynamics that are well-known to supply growing season moisture in this region.

2.3. Paleoclimate Reanalysis

To complement the analysis of the tree-ring soil moisture reconstruction, we also used the Paleo Hydrodynamics Data Assimilation (PHYDA) product (Steiger et al., 2018). PHYDA is a global, gridded, ensemble reconstruction of a variety of climate variables for the entirety of the Common Era. PHYDA is constructed using a data assimilation approach with nearly 3,000 paleoclimate proxies and simulations from a general circulation model (the Community Earth System Model Last Millennium Ensemble; CESM-LME). Variables in PHYDA have monthly, seasonal, or annual temporal resolutions, and include various climate indices (e.g., Niño 3.4), surface air temperatures, and drought indices. PHYDA has been used successfully in several applications relevant for our study, including analyses of drought variability in western North America (Steiger et al., 2019), hydroclimate responses to volcanic events (Tejedor et al., 2021), and concurrent megadroughts in North and South America (Steiger et al., 2021). Notably, hydroclimate variability reconstructed in PHYDA for our region of interest, and western North America more broadly, compares favorably with other reconstructions (Steiger et al., 2019).

We used the PHYDA primarily to extend our analysis of ocean forcing of droughts and pluvials in the SWNA region beyond the instrumental record, using both the PHYDA ensemble mean and the 100-member subset of the PHYDA ensemble generated by the reconstruction. For hydroclimate, we used the PHYDA summer season (JJA) Palmer Drought Severity Index (PDSI) averaged over SWNA. PDSI from the PHYDA has a continuous, millennial-length linear trend toward wetter conditions that is absent in SM-REC. To generate estimates of droughts and pluvials in PHYDA comparable to SM-REC, and because we are not focused on trends in our analyses, we linearly detrend the PHYDA PDSI and rescale it to match the mean and variance of SM-REC over the full overlapping period (800–2000 CE). With this processing, the relationship between SM-REC soil moisture and ensemble mean PHYDA PDSI is highly linear, with a strong and highly significant ($p \leq 0.001$) positive correlation (Pearson's $r = +0.89$) (Figure S3 in Supporting Information S1).

For climate indices, we use the PHYDA provided indices for DJF Niño 3.4 and JJA AMO. We calculate our own PDO index from PHYDA as the first principal component of DJF seasonal average surface air temperatures in the Pacific basin north of 20°N (Mantua et al., 1997; Newman et al., 2016). As with the original PHYDA PDSI, centennial-scale variations and long-term trends are extant in these PHYDA climate indices but absent in the associated instrumental SST indices. To generate time series comparable with their instrumental counterparts, PHYDA indices were detrended using a 100-year lowess spline and scaled to match the mean and variance of the

seasonal instrumental climate indices over the period 1901–2000. This processing removed any long-term trends while retaining the strong decadal to multi-decadal variability also present in the instrumental data. Across the PHYDA ensemble, the median correlation with the observed DJF Niño 3.4 record for the 20th century (1901–2000) is 0.751 (ensemble range: 0.742–0.756). Results are weaker for the PDO (median: 0.426; range: 0.416–0.439) and AMO (median: 0.419; range: 0.405–0.425), though this may reflect the low-frequency nature of these modes. Indeed, when the observed and PHYDA-based indices are smoothed with a 10-year lowess filter, the correlations improved markedly for both the PDO (median: 0.778; range: 0.749–0.812) and AMO (median: 0.620; range: 0.590–0.636).

2.4. Identifying Extended Droughts and Pluvials

For our analyses, we focus on the most persistent drought and pluvial events in SM-REC and PHYDA, leveraging the methodology of Williams et al. (2020, 2022) which is designed to find the most persistent, multi-year events (referred to here as "extended" droughts and pluvials). Soil moisture time series were first smoothed with a 10-year trailing running-mean. Strings of years with 10 or more smoothed values below zero were initially identified as droughts, while strings of years with 10 or more smoothed values above zero were identified as pluvials. All the unsmoothed values used in the calculation of these running means were then used as the potential range of years for each drought or pluvial. From these unsmoothed values, values were trimmed from either end to ensure droughts and pluvials met several criteria. Droughts were required to begin with two consecutive negative values, terminate with two consecutive positive values, and never end on a positive value. Pluvials were required to begin with two consecutive positive values, terminate with two consecutive negative values, and never end on a negative value. We then excluded any of these events less than 5 years in duration, and included any periods with 5 consecutive annual negative (droughts) or positive (pluvial) soil moisture anomalies that were not identified in the initial criteria. These constraints ensure that we are identifying the most persistent drought and pluvial events and minimizing the influence of singular wet years on droughts or singular dry years on pluvials. For all events, we calculate and evaluate their *duration* (total number of years in the event) and *severity* (cumulative sum of all anomalies during the event in units of σ).

2.5. Bayesian Hierarchical Modeling

To determine the importance of SST forcing for droughts and pluvials, we use a Bayesian structural time series model where the value of soil moisture S_t at any given time is predicted by a weighted linear combination of soil moisture in the two preceding years and current SST indices T_t^j:

$$S_t \sim N\left(\rho_1 S_{t-1} + \rho_2 S_{t-2} + \sum_{j=1}^{n_{index}} \beta^j T_t^j, \tau\right) \tag{1}$$

We use PHYDA-reconstructed Niño3.4, AMO, PDO indices and JJA global mean temperature for the covariates T^j. These SST indices are themselves uncertain; to take this into account we use a hierarchical model in which the "true" (latent) value of the index T^j is estimated from the 100-member ensemble generated by the PHYDA reconstruction. We assume each ensemble member $\hat{T}_t^j$ can be modeled by

$$\hat{T}_t^j \sim N\left(T_t^j, \tau_t^j\right) \tag{2}$$

where τ_t^j is the time-dependent ensemble standard deviation for SST index j. This allows us to take into account the fact that the reconstructed SST indices are less certain earlier in the record. We place $N(0,1)$ priors on the lag coefficients ρ_1 and ρ_2, broader $N(0,10)$ priors on the coefficients β^j, and a half normal prior with width 10 on the white noise term τ. We then use Markov Chain Monte Carlo sampling to determine the posterior distributions. We train this model on pre-industrial (800–1849) PHYDA and soil moisture reconstructions and then assess its ability to predict out-of-sample recent (1850–2000) soil moisture given recent SST indices from PHYDA.

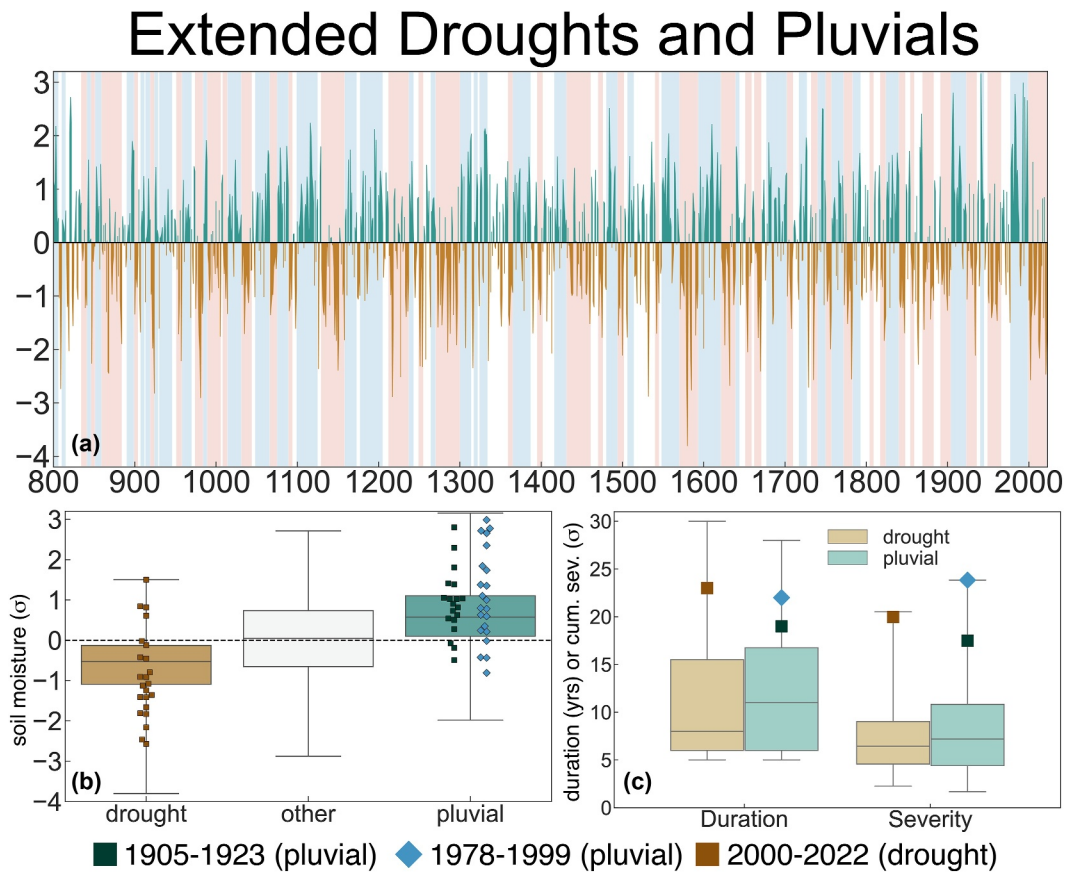

Figure 1. (a) SM-REC time series of Southwestern North America summer (JJA) soil moisture (σ) with extended droughts (red) and pluvials (blue) highlighted. (b) Boxplots of soil moisture during all extended droughts ($n = 463$), pluvials ($n = 488$), and other years ($n = 273$). Note that wet years can occur during droughts and similarly dry years can occur during pluvials because the initial filtering for these events is based on 10-year trailing mean averages. Overlaid swarm plots are individual years from the 20th-century pluvials and early 21st-century megadrought (see legend). (c) Boxplot comparisons of duration (years) and cumulative severity (absolute magnitude, σ) during all identified droughts and pluvials, with major recent events (1905–1923 and 1978–1999 megapluvials; 2000–2022 megadrought) indicated by the box and diamond icons.

3. Results

3.1. Extended Droughts and Pluvials

We identified 39 extended droughts and 38 extended pluvials in the SM-REC soil moisture reconstruction from 800 to 2023 CE (Figure 1a; Tables S1 and S2 in Supporting Information S1). These include well known drought events highlighted in other studies including the Ancestral Puebloan drought in the 13th century (1271–1300) (Benson et al., 2007), the late 16th-century megadrought (1571–1593) (Fye et al., 2003), and the Colorado River Basin drought of the mid-1100s (1130–1158) (Meko et al., 2007). Similarly, our pluvial algorithm picked out major pluvials, including events in the mid-16th century (1549–1570) (Fye et al., 2003), the early 1600s (1594–1621) (Robeson et al., 2020), and the early 1800s (1825–1840) (van der Schrier & Barkmeijer, 2007). The majority of years in the record ($n = 951$, 77.7% of all years) were nearly equally distributed between the droughts ($n = 463$, median= -0.52σ) and pluvials ($n = 488$, median= $+0.58\sigma$) (Figure 1b).

Our analysis places the early and late 20th-century pluvials at 1905–1923 and 1978–1999, respectively. Applying our broad definition of *megapluvials* as especially extreme wet events (adapted from the megadrought definition in B. I. Cook et al. (2022)), both 20th century events would qualify as *megapluvials* (Figure 1c). The early 20th-century megapluvial is the 8th longest in the 1,224 years record (19 years), ranking as the second most severe in terms of cumulative severity ($+17.49\sigma$). The late 20th-century megapluvial is even more extreme, standing as the

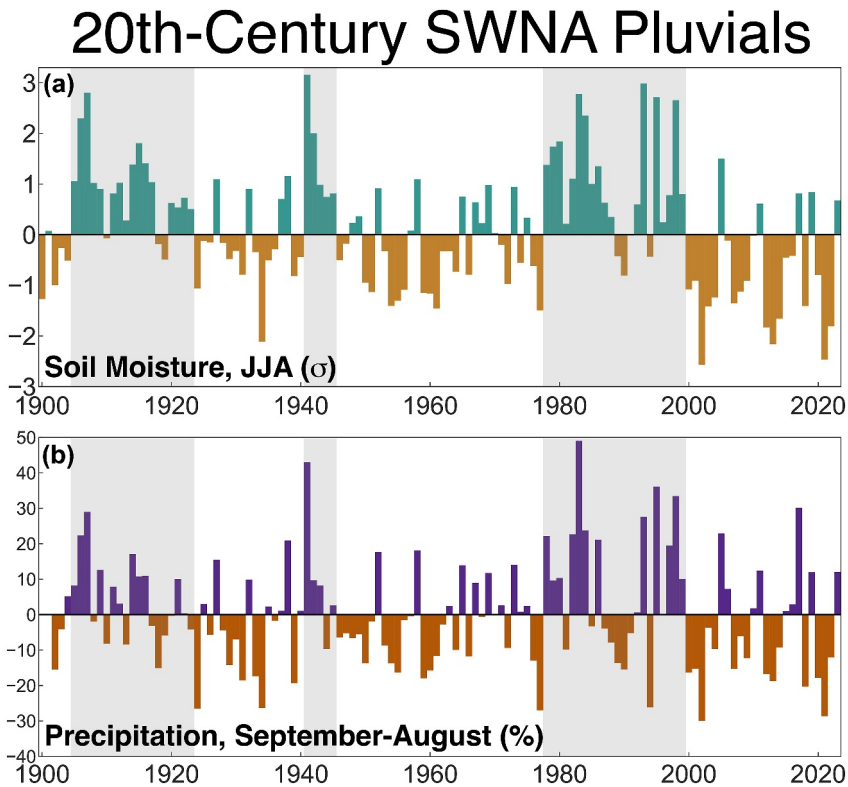

Figure 2. (a) SM-REC time series of Southwestern North America summer (JJA) soil moisture (σ) with 20th century pluvials highlighted in gray: 1905–1923, 1941–1945, and 1978–1999. (b) Same as panel (a), but for September–August precipitation anomalies (%, relative to baseline of 1901–2023).

fifth longest (22 years) and first most severe pluvial in the record (+23.83σ). In terms of absolute severity, these megapluvials are comparable to the early 21st-century megadrought (23 years; 2000–2022) (−19.97σ).

3.2. Precipitation and Ocean Forcing of the 20th-Century Megapluvials

The 20th-century megapluvials (1905–1923 and 1978–1999), along with a shorter pluvial in the 1940s (1941–1945), are highlighted in the SM-REC soil moisture and preceding 12-month (September–August) precipitation anomalies in Figure 2. The extreme and persistent wetness during the megapluvials clearly stands out compared to the rest of the century, though both megapluvials had multi-year periods of precipitation deficits (1917–1920 and 1987–1992). These dry intervals did not terminate the pluvials in our algorithm because the 10-year moving window soil moisture remained positive. The 1978–1999 megapluvial was immediately followed by the early 21st-century megadrought (2000–2022). Similar to the megapluvials, the early 21st-century megadrought also had brief periods when precipitation anomalies were in opposition (wet) to the mean conditions (dry) during the event.

While both megapluvials were driven by extended surpluses in total precipitation, the seasonal and geographic distribution of precipitation differed markedly between the two events (Figure 3). Fall was generally dry during the 1905–1923 megapluvial and the event actually ended with a cumulative net deficit in SON precipitation averaged over SWNA (Figure S4 in Supporting Information S1). Winter was the single wettest season of this megapluvial, with the full 19-year cumulative precipitation anomaly for DJF ranking as the highest compared to all other (overlapping) 19-year periods in the record (Figure S4 in Supporting Information S1). More modest absolute precipitation surpluses occurred during MAM and JJA, consistent with results from previous analyses of this event (B. I. Cook et al., 2011).

Positive precipitation anomalies were much more widespread and consistent across seasons during the more recent 1978–1999 megapluvial. During this event, cumulative 22-year precipitation anomalies for both DJF and MAM over SWNA were near record breaking, while both SON and JJA ranked in the top 20% (Figure S4 in

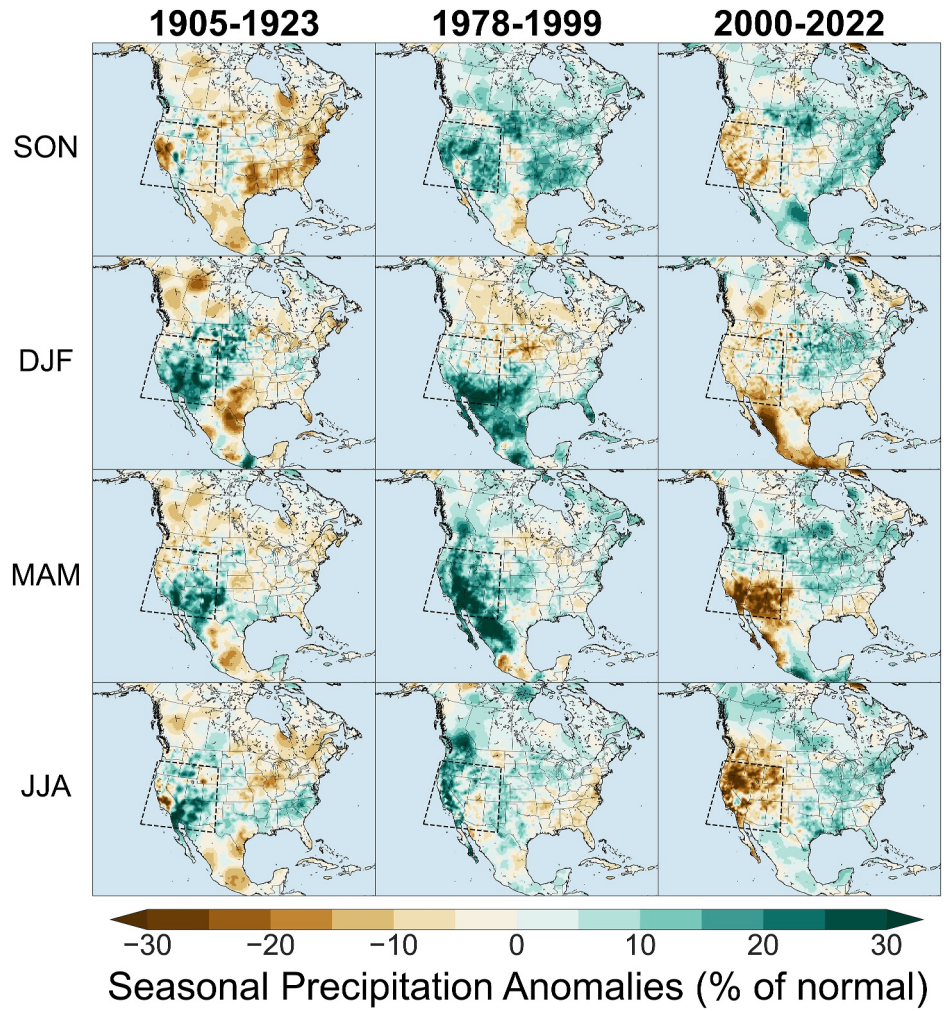

Figure 3. Seasonal precipitation anomalies (%) during the early 20th-century megapluvial (1905–1923; left column), late 20th-century megapluvial (1978–1999; center column), and early 21st-century megadrought (2000–2022; right column). Baseline period for the anomaly calculation is 1901–2022. Dashed box represents the Southwestern North America region, the area of focus for our analyses.

Supporting Information S1). This anomalous wetness was especially widespread during the spring, extending across western North America from Mexico into western Canada. This was similar to the seasonality of the precipitation *deficits* during the 2000–2022 megadrought, which were also substantial and extant in all seasons (Figure S4 in Supporting Information S1).

The spatial patterns of the precipitation anomalies during these events show some similarities to the canonical precipitation responses to Pacific and Atlantic SST forcing, suggesting a possible role for these climate modes. For example, positive precipitation anomalies across western North America are favored by warm anomalies in the tropical Pacific (El Niño or positive phases of the PDO) and colder than average SSTs in the tropical Atlantic (negative phases of the AMO) (Figure S5 in Supporting Information S1) (S. Schubert et al., 2009). These SST event composites are similar to the observed precipitation anomalies for 1978–1999 (Figure 3), which bear strong resemblance to what would be expected during El Niño (in DJF and MAM) and positive PDO (in MAM) events. This includes a zonally extensive band of positive precipitation anomalies across Mexico and the southern United States in DJF and wetter than normal conditions covering nearly all of western North America from Mexico up through northwest Canada in MAM. These anomalies are also broadly consistent with a negative AMO pattern, including during SON and JJA. By contrast, precipitation anomalies are less consistent with these forcing patterns and more highly localized during the 1905–1923 megapluvial. For example, MAM precipitation surpluses during 1905–1923 are largely confined to SWNA, and SON shows substantial deficits across much of North America.

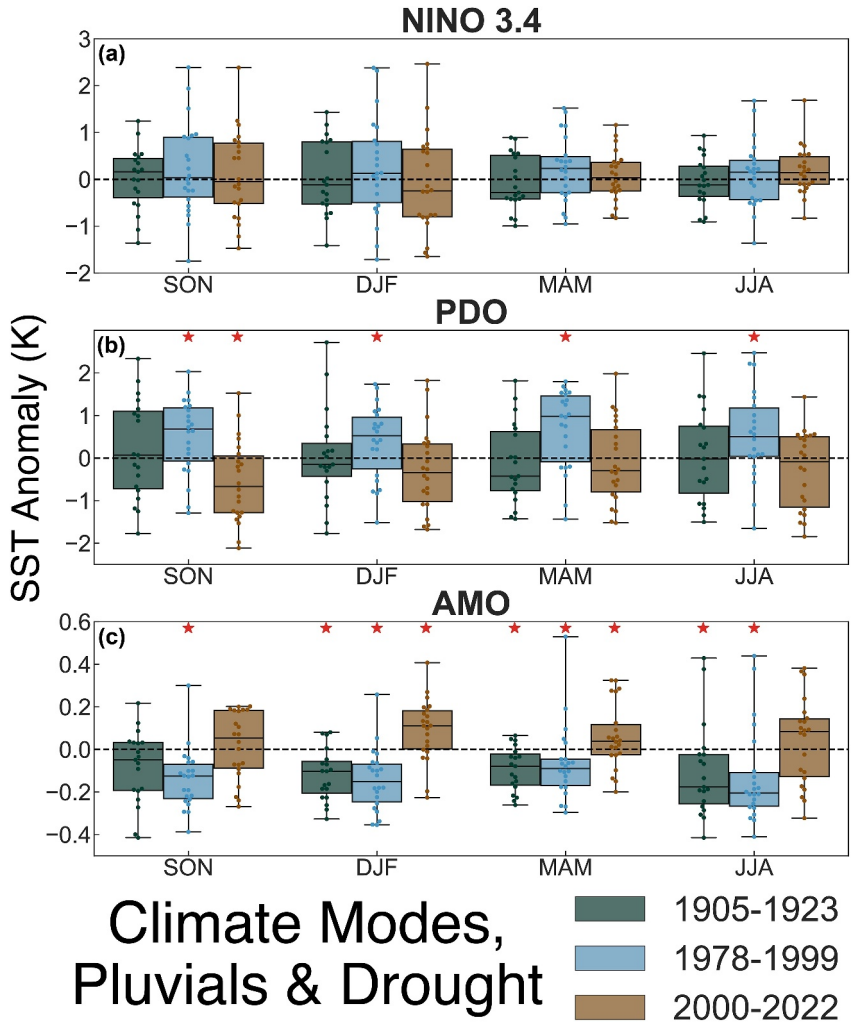

Figure 4. Seasonal SST anomalies (K) associated with Pacific (Niño 3.4 Index, Pacific Decadal Oscillation) and Atlantic (Atlantic Multidecadal Oscillation) climate modes. Red stars indicate distributions that are significantly different (Two-sided Kolmogorov-Smirnov test, $p \leq 0.05$) from all other anomalies taken from the full period of record used for the climate modes (1871–2023).

Evidence for stronger SST forcing during the 1978–1999 pluvial can also be seen in comparisons of the observed (Figure S6 in Supporting Information S1) and SST composited (Figure S7 in Supporting Information S1) 200 hPa height anomalies. Strong negative height anomalies were centered over the North Pacific and southeastern United States during DJF and MAM in 1978–1999. These circulation patterns are similar to what would be expected during El Niño events, positive phases of the PDO, and (to a lesser extent) negative phases of the AMO. These SST composites and the observed anomalies during 1978–1999 show a strong low-pressure anomaly over the North Pacific during DJF and MAM, which would favor advection of moisture and tracking of storms into western North America. By contrast, 1905–1923 height anomalies are much weaker in magnitude and lack the large-scale coherence that is evident in the SST composites, supporting the hypothesis of weaker ocean forcing during this event. Explicitly attributing the pluvials to these individual forcing modes using this qualitative analysis is undermined, however, by the limited sampling and substantial overlap in years across modes when constructing these composites. This is especially an issue regarding the PDO and AMO, modes of variability with significant power at lower frequencies limiting the degrees of freedom available from the short instrumental record. We explore the role of SST forcing during these pluvials in a more quantitative framework using our Bayesian modeling approach with the PHYDA reconstruction, which we describe later.

Distributions for the SST-based climate indices further highlight differences in forcing across these events (Figure 4). To assess whether the climate indices were significantly ($p \leq 0.05$) shifted positive or negative during the pluvials or drought, we compare all years during each event to all other years in the record using a two-sided Kolmogorov-Smirnov test. Somewhat surprisingly, none of the three events analyzed (1905–1923 and 1978–1999 megapluvials; 2000–2022 megadrought) show significant shifts in the distribution of the Niño 3.4 index in any season (Figure 4a). This does not preclude the potentially important contributions from several strong El Niño events (e.g., 1982/1983, 1997/98) during the 1978–1999 megapluvial. However, Pacific ocean forcing appears to have manifested much more strongly in the PDO index for this event (Figure 4b), which shows significant shifts toward positive conditions in all four seasons. By contrast, PDO shifts are not significant in any season for the early 20th century megapluvial and only for SON during the early 21st century megadrought. These results are consistent with previous analyses by McCabe et al. (2004) that show much stronger positive PDO forcing during the latter versus early decades of the 20th century. Shifts in the AMO are much more common across the three hydroclimate events (Figure 4c). The 1978–1999 megapluvial has significant colder AMO conditions in all four seasons; similar shifts occur during 1905–1923 in DJF, MAM, and JJA. These results are also consistent with the analysis of McCabe et al. (2004) that showed extended negative AMO conditions during the decades encompassing these two pluvials. The early 21st-century megadrought also shows significant shifts toward warmer AMO conditions in DJF and MAM, favoring drier conditions during this event.

3.3. Pluvial and Megapluvial Variability Over the Last Millennium

We identified 30 pluvials and 29 droughts in the PHYDA ensemble mean (Figure S8a in Supporting Information S1; Tables S3 and S4 in Supporting Information S1), fewer than in SM-REC but with substantial temporal overlap in the events shared between the two data sets. These include the 13th (SM-REC: 1271–1300; PHYDA: 1270–1300) and 16th (SM-REC: 1571–1593; PHYDA: 1570–1586) century megadroughts; the 1825–1840 pluvial (same years in both data sets); and both the early 20th-century (SM-REC: 1905–1923; PHYDA: 1901–1923) and late 20th-century (1978–1999 in both data sets) megapluvials. As in SM-REC, the 20th-century megapluvials in PHYDA stand out as similarly extreme (Figure S8b in Supporting Information S1). In PHYDA, the 1901–1923 megapluvial now emerges as the single most extreme pluvial in the record (cumulative severity $+26.54\sigma$), while the 1978–1999 event drops to fifth most severe ($+19.41\sigma$). Such differences between the two records are not surprising, given the differences in methodologies, observations, and proxy networks employed by the two data sets. However, the general agreement between the two data sets on the extreme nature of the 20th-century megapluvials suggests this is a robust result.

Consistent with the analysis of SM-REC and the observed climate indices, the PHYDA shows stronger positive (warm) tropical Pacific conditions during the late 20th-century megapluvial compared to the early 20th-century event (Figure 5). More generally, the PHYDA reproduces the expected relationship between SWNA hydroclimate and tropical Pacific forcing observed in other analyses of instrumental and tree-ring based PDSI (Baek et al., 2017). Across all years (800–2000 CE) in the PHYDA ensemble, Pearson's r between SWNA JJA PDSI and DJF PDO is +0.68 (same for instrumental period 1871–2000); with DJF Niño 3.4 the correlation is +0.40 (+0.25 for 1871–2000). Comparisons of the PDO and NINO 3.4 indices during all identified droughts and pluvials across all years in the entire PHYDA ensemble show a similar (positive) relationship between tropical Pacific forcing and SWNA hydroclimate (Figure 6).

However, the expected relationship from observations between the AMO and SWNA soil moisture does not appear to hold in the PHYDA for the late 20th-century megapluvial (Figure 5), or more generally for droughts and pluvials in the full record (Figure 6). Observations show an inverse relationship between tropical Atlantic SSTs and hydroclimate in SWNA (warm SSTs = drought) (Baek et al., 2017; McCabe et al., 2004), and for 1871–2000 the Pearson's correlation between SWNA PDSI and the JJA AMO index across the PHYDA ensemble reflects this (−0.09). Over the full period of record in the PHYDA ensemble (800–2000), however, the sign of the correlation is actually reversed (+0.21). This highlights the uncertainty in the role of the AMO for forcing SWNA hydroclimate, in the PHYDA at least.

It is difficult to ascribe this inconsistency between the PHYDA and observations to a particular cause. One possibility is that the limited sampling during the instrumental era may be biasing our interpretations of the role of Atlantic SSTs in North American hydroclimate: since the mid-1800s, only about two and one half cycles of the AMO have occurred (Triacca & Pasini, 2024). These interpretations may be further confounded by evidence that

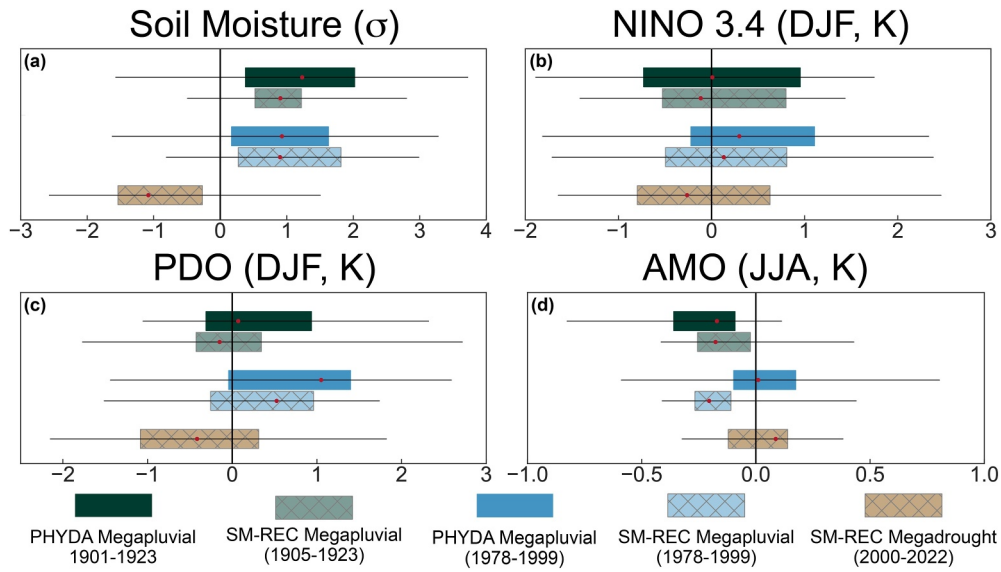

Figure 5. Box and whisker plot comparisons between SM-REC, the observed SST indices, and the PHYDA for the 20th-century megapluvials and 21st-century megadrought. For the PHYDA, plots include combined information from calculations across each of the 100 individual ensemble members. (a) Soil moisture (σ), (b) DJF Niño 3.4 index (K), (c) DJF PDO index (K) and (d) JJA AMO index (K).

multi-decadal SST variability in the Atlantic is at least partially driven by natural (volcanic) and anthropogenic (aerosol) forcing (Mann et al., 2021; Qin et al., 2020). The weaker and inverted relationship between the AMO and SWNA hydroclimate in the PHYDA could also be a consequence of the climate model (CESM) providing the

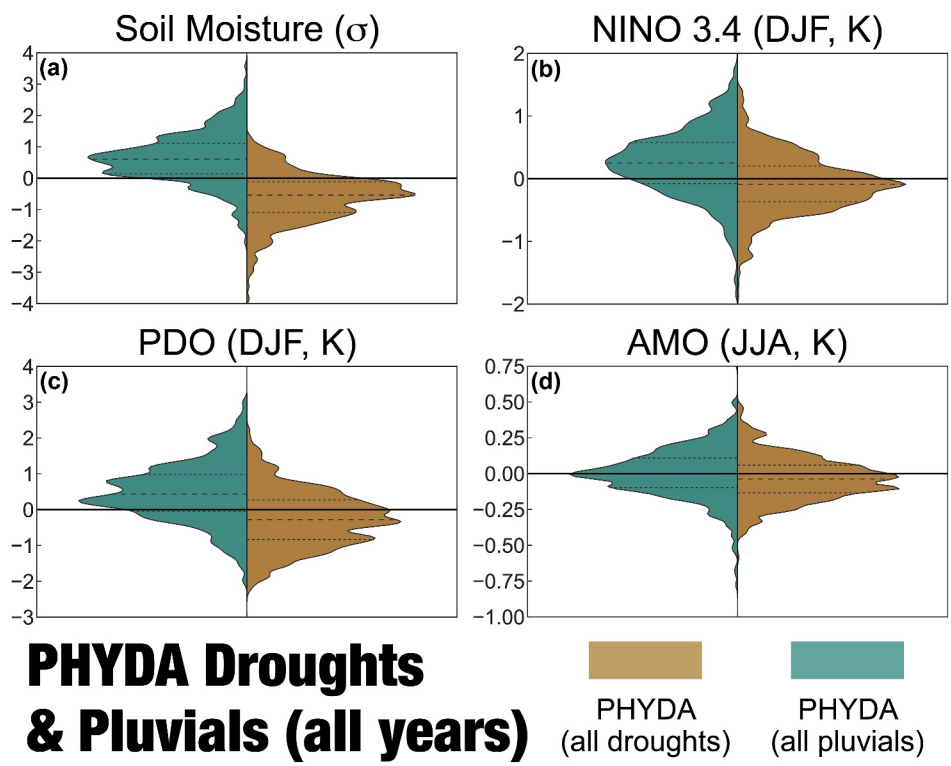

Figure 6. Distributions of panel (a) soil moisture (σ), (b) DJF Niño 3.4 index (K), (c) DJF PDO index (K) and (d) JJA AMO index (K) during all drought and pluvial years from the full 100-member PHYDA ensemble. Dashed lines in the distribution delineate the quartiles in the data.

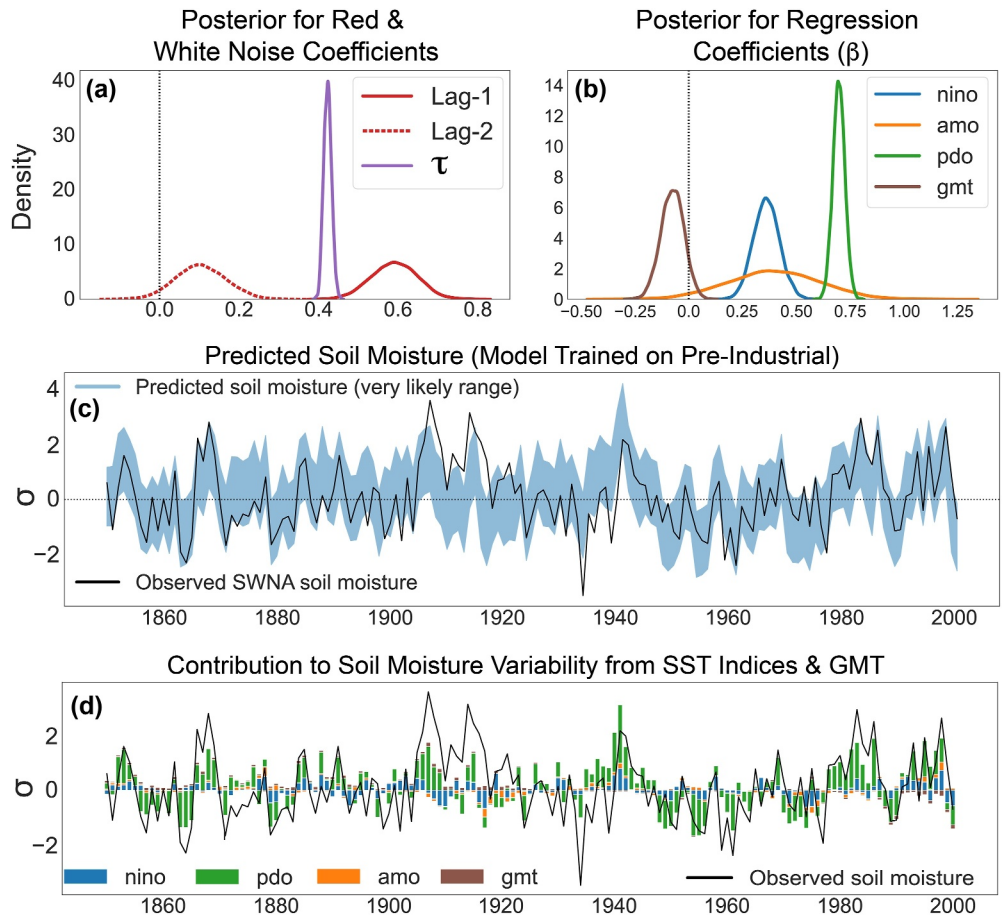

Figure 7. (a) Posterior distributions for the lag-1 and -2 coefficients and the white noise τ. (b): Same, but for the regression coefficients β^j. (c) Predicted recent (1850–2000) soil moisture using the model trained on preindustrial soil moisture and SSTs (95% highest posterior density interval, blue) compared to observations (black line). (d) Contributions of each temperature index to observed soil moisture. Bars indicate the posterior mean.

dynamical constraints for the reconstruction. Over 1871–2000, the Pearson's correlation between the instrumental DJF Niño 3.4 index and the following JJA AMO index is −0.19. For the same period in the PHYDA, the Pearson's r is +0.32. This indicates, in PHYDA, a tendency for warm tropical Atlantic SSTs to occur with the warmer tropical Pacific SST states that would drive wetter than normal conditions in SWNA. There may also be intrinsic non-stationarities in the connections between Pacific and Atlantic SSTs and North American hydroclimate over the last millennium. Additionally, the large region over which we are considering soil moisture may be affecting the interpretation of the teleconnections by smoothing or averaging out local scale signals across space. This can be seen, for example, in the composite event plots (Figure S5 in Supporting Information S1) that show a shift in the sign of the ENSO precipitation response between the southern and northern half of SWNA during DJF.

3.4. Bayesian Modeling and Likely Causes of the Late 20th Century Megapluvial

We applied our Bayesian hierarchichal model, trained on the pre-industrial portion of the PHYDA, to better quantify the drivers of the 20th-century megapluvials. Figure 7a shows the posterior distributions for the lag-1 and lag-2 coefficients, as well as the white noise term τ. The soil moisture depends strongly on its value in the previous year, and weakly on its value 2 years prior. Figure 7b shows the posteriors for the coefficients β associated with the individual SST indices and global mean temperature. Nearly all the posterior mass for β^{nino} (blue line) is positive, indicating that a positive Niño 3.4 is virtually certain to be associated with wetter soil moisture. The same is true of the PDO (green line), although this relationship is both stronger and more confident than the Niño 3.4 dependence. As discussed above, the AMO (orange line) is positively correlated with soil moisture, although the

broad width of the posterior distribution indicates low confidence in the magnitude of this relationship. Finally, higher global mean temperatures appear to be associated with drier soil moisture (brown line), although the relationship over the pre-industrial era is weak and less certain, consistent with previous analyses of the PHYDA (Steiger et al., 2019).

We can use these posterior distributions to predict out-of-sample soil moisture over 1850–2000. Blue shading in Figure 7c shows the resulting 95% highest posterior density interval for the predicted soil moisture. When compared to the observations (black line), it is evident that the model trained on pre-industrial data is quite skillful in capturing the observed variability. This suggests that the relationships between SSTs and soil moisture over the Common Era continued to hold over the 20th century. Figure 7d shows the posterior mean contribution of each SST index and global mean temperature to SWNA JJA soil moisture in each year. Specifically, the stacked bar plots represent the aggregate summer soil moisture response to the SST indices in the model, which can be compared with the observed soil moisture (black line) to assess the contributions of SST forcing. For example, in a year where the green bar (representing the PDO) is equal in magnitude to the black line, this indicates the model response to PDO forcing in this year can explain the entirety of the observed soil moisture response. Conversely, where the magnitude of the stacked bar is much less than the black line, the SST forcing, as represented in our model, is not estimated to be a major contributor to the soil moisture anomaly.

As can be seen in Figure 7d, the relative contributions of SST forcing to the soil moisture anomaly can widely vary from year to year. The 1978–1999 megapluvial is largely explained by the SST forcing, indicated by the fact that the cumulative bar plots are nearly equal in magnitude to the observed values for most years of this event. This is driven primarily by the PDO, with minor contributions from the AMO and Niño 3.4 during the latter half of this event. This stands in sharp contrast with the early 20th-century pluvial, which is poorly explained by the SST forcing, as indicated by the large gap between the observed soil moisture and stacked bar plot during these years.

Notably, the Bayesian model suggests a much weaker contribution of the AMO to the megapluvial events when compared to the observed SST analysis in Figure 4, a discrepancy that could arise from a range of reasons. The Bayesian model is trained on the pre-industrial period in the PHYDA, using a data set and time period where the AMO teleconnection to drought over SWNA is much weaker. Whether this reflects deficiencies in the PHYDA reconstruction or non-stationarities in AMO dynamics and regional teleconnections is unclear. Regardless of the cause, these issues are reflected in the larger uncertainty in the posterior for the AMO β coefficient in the model (Figure 7b). Alternately, the strong coherence between the AMO and the 20th-century megapluvials in Figure 4 may simply be a coincidence. Robust analyses of multi-decadal variability in the 20th century are difficult because of the limited sampling of these events. As discussed previously, there is also at least some evidence that the AMO may not even be a robust mode of internal climate variability. Indeed, one motivation for using the PHYDA was to allow for a broader, longer-term analysis of the role of these SST modes in hydroclimate variability over SWNA.

4. Discussion and Conclusion

Using a 1,224 years long record of soil moisture constructed from observations and tree-ring estimates, we demonstrate that multi-year pluvials are as ubiquitous, persistent, and extreme as droughts over the last millennium of hydroclimate variability in SWNA. This includes the occurrence of "megapluvials", wet periods that, like megadroughts, are distinguished by their exceptional severity or persistence. Two such megapluvials occurred near the beginning (1905–1923) and end (1978–1999) of the 20th century, events with profound implications for water resources, people, and ecosystems across western North America. As with droughts, extended pluvials in SWNA are strongly linked with SST variability in the tropical Pacific, though the importance of this forcing can vary substantially between events. Our Bayesian model provides strong evidence that warm SSTs in the tropical Pacific were the primary driver of the record-breaking late 20th-century megapluvial, while suggesting SST forcing played a much more limited role during the early 20th century event. These results corroborate independent findings using climate model experiments, which have also demonstrated the much stronger role for SST forcing during the late versus early 20th-century megapluvial (B. I. Cook et al., 2011; H.-P. Huang et al., 2005; Seager et al., 2023).

We find the role of warm tropical Atlantic SSTs during pluvials to be much more uncertain, with notable inconsistencies in the relationships between the AMO and SWNA hydroclimate across observations and the PHYDA. It is possible that the role of the AMO during these pluvials is stronger than our Bayesian model would

indicate. Indeed, tropical Atlantic SSTs have been widely connected to a variety of major hydroclimate extremes over North America and elsewhere in the paleoclimate (Oglesby et al., 2012; Thirumalai et al., 2018) and observational (Kushnir et al., 2010; McCabe et al., 2004; Ting et al., 2011) records. Other studies, however, have found the influence of Atlantic SSTs on North American droughts to be limited (Baek, Smerdon, et al., 2019; Baek, Steiger, et al., 2019). Our current understanding of the dynamics, variability, and stationarity of low-frequency Atlantic SST variability, and its impact on terrestrial hydroclimate, therefore remains poor. Future advances would benefit from expanded estimates of Atlantic SST variability in the paleoclimate record.

Our findings highlight the continuing importance of SST variability for hydroclimate in SWNA, even in the face of climate change driven trends toward aridification (B. I. Cook et al., 2021; Williams et al., 2022). The importance of such patterns for future drought and pluvial events, however, will likely depend on the extent to which this ocean variability is forced versus internally generated. As discussed previously, there is increasing evidence that recent shifts in the AMO and tropical Atlantic SSTs are being driven by natural and anthropogenic forcings (Mann et al., 2021; Qin et al., 2020). The same may be occurring in the Pacific as well. For example, Hua et al. (2018) ascribed tropical Pacific warming in the 1990s to greenhouse gas warming and recovery from volcanic eruptions, and similarly suggested that cooler Pacific SSTs post-1998 were at least partially driven by anthropogenic aerosols. Distinguishing between internal versus forced components of these important modes of hydroclimate variability in SWNA will be critically important to understand the role they will play in the future.

Several of our methodological choices are likely to affect our interpretations and conclusions. We used 200-cm soil moisture in our analyses, but hydroclimate variability can be quantified using other hydrologic variables with their own intrinsic timescales and process sensitivities. Soil moisture generally has much longer interseasonal and interannual memory than precipitation and is more sensitive to changes in evaporative demand than streamflow or runoff (Mankin et al., 2019). The extent to which our conclusions and interpretations regarding the frequency, duration, and intensity of pluvials generalizes to these other variables is therefore an open question. We also focused specifically on extended, multi-year events at least 5 years in duration. However, the processes that drive shorter term events (e.g., internal atmospheric variability) are likely to be different from the forcings responsible for more persistent, multi-year droughts and pluvials (e.g., tropical SSTs). As a result, our conclusions regarding the drivers of pluvials may not necessarily hold for shorter-term wet extremes, such as the near-record wet 2023 winter in California (S. D. Schubert et al., 2024). Finally, we note that the algorithm we used to identify drought and pluvial periods is just one of many in the literature (B. I. Cook et al., 2022). There is no singular accepted method for defining the onset and termination of multi-year droughts and pluvials, and alternative approaches will generate different results. The algorithm we employ is designed to identify only the most persistent dry or wet intervals, and specifically minimize the influence of dry years on pluvials and wet years on droughts.

While arguably overlooked in the scientific literature compared to major droughts in the instrumental-era, the ecological and societal importance of the 20th-century megapluvials in western North America is clear. Almost half (41 years) of the 20th century was encompassed by these events, and the associated increases in water availability helped facilitate the rapid economic, agricultural, and ecological growth in the West during these decades. These megapluvials may have therefore created a false sense of security, one that would be immediately undermined by extreme droughts that followed in the 1920s and 1930s (Woodhouse et al., 2020) and the early 21st century (Williams et al., 2022). Such sharp, decadal swings in moisture may have even contributed to biased perceptions of the climate in western North America in the early 19th century. Observations from several expeditions, most famously the one led by Zebulon Pike, helped form the dominant narrative of the West as the "Great American Desert" (Culver, 2012; Morris, 1926). These reports were based on periods identified in our analysis as major droughts (1805–1809 and 1818–1824). By contrast, competing accounts suggesting much more mesic conditions in the region emerged in the 1840s, based largely on John Charles Frémont's 1842 expedition (Culver, 2012; Menard, 2011). Here too, however, perceptions may have been biased by the immediately preceding 1825–1840 pluvial. Given this, it may therefore be more appropriate to characterize the West less as a region that is "drought prone", and more one where "pluvial-drought" whiplash on decadal timescales is a defining feature.

More practically, pluvials are critically important for the restoration of natural (e.g., groundwater, streamflow, soil moisture) and anthropogenic (e.g., surface reservoirs) water resources depleted during droughts (Alam et al., 2021). Their importance may be further amplified in regions like SWNA, where climate change is expected to increase drought risk and severity with warming (B. I. Cook et al., 2015, 2020, 2021). Our results suggest that

pluvials, including the record-breaking 1978–1999 megapluvial, are often driven by strong forcing from warm tropical Pacific SSTs. This highlights the possibility that similar patterns would cause pluvials in the future, potentially providing at least some relief in the region. However, such a pluvial would occur in a warmer world where anthropogenic forcing will have a larger impact on the processes affecting soil moisture availability. In SWNA, this is most likely to occur through warming driven increases in evaporative demand and snow melt, resulting in drier soils (B. I. Cook et al., 2021; Williams et al., 2022) and reducing the efficacy of wet periods to terminate droughts and restore water resources (Nielsen et al., 2024). This was demonstrated recently in Seager et al. (2023), who used SST-forced climate model ensembles to demonstrate that, even under the most favorable ocean conditions for pluvials (positive PDO, negative AMO) over the next two decades (out to 2040), models cannot reproduce the magnitude of the late 20th century pluvial. There is thus a clear imperative to improve our understanding of how pluvials in the future may compare to pluvials in the past, including their role in water resources and hydroclimate dynamics in a warming world.

Conflict of Interest

The authors declare no conflicts of interest relevant to this study.

Data Availability Statement

Niño 3.4 index: https://psl.noaa.gov/data/timeseries/month/ [Dataset]; PDO Index: https://www.ncei.noaa.gov/monitoring-content/teleconnections/pdo/data/ersst.v5.pdo.dat [Dataset]; AMO Index: https://climexp.knmi.nl/getindices.cgi?WMO=UKMOData/amo_hadsst [Dataset]; Precipitation Data: https://www.ncei.noaa.gov/access/metadata/landing-page/bin/iso?id=gov.noaa.ncdc:C00332 [Dataset] (Vose et al., 2014); SM-REC https://zenodo.org/records/13755272 [Dataset] (Williams, 2024); PHYDA Ensemble Average https://zenodo.org/records/1198817 [Dataset] (Steiger, 2018); PHYDA Ensemble Members https://clifford.ldeo.columbia.edu/nsteiger/recon_output/phyda_ens/ [Dataset] (Steiger, 2018). Analyses and figures produced using the following modules in python 3 (Van Rossum & Drake, 2009) [Software]: calendar (no reference available) [Dataset], datetime (no reference available) [Dataset], os (no reference available) [Dataset], numpy (Harris et al., 2020) [Dataset], netCDF4 (no reference available) [Dataset], copy (no reference available) [Dataset], matplotlib (Hunter, 2007; Team, 2024) [Dataset], scipy (Virtanen et al., 2020) [Dataset], seaborn (Waskom, 2021) [Dataset], pandas (Wes McKinney, 2010; pandas development team, 2020) [Dataset], statsmodels (Seabold & Perktold, 2010) [Dataset], IPython (Pérez & Granger, 2007) [Dataset], requests (no reference available) [Dataset], cartopy (Met Office, 2010 - 2015) [Dataset], shapely (Gillies, 2007) [Dataset], pymc (Abril-Pla et al., 2023) [Dataset], and arviz (Kumar et al., 2019) [Dataset]. All analysis code available from https://zenodo.org/records/13799310 (B. Cook & Marvel, 2024) [Software].

Acknowledgments
JES and RS were supported by NSF award AGS-2101214. RS was additionally supported by NSF award AGS-2127684. APW supported by the USGS Southwest Climate Adaptation Science Center (USGS 314653-00001, G24AC00611). BIC and KM supported by NASA's Modeling, Analysis, and Prediction program.

References

Abril-Pla, O., Andreani, V., Carroll, C., Dong, L., Fonnesbeck, C. J., Kochurov, M., et al. (2023). PyMC: A modern, and comprehensive probabilistic programming framework in Python [Software]. *PeerJ Computer Science*, *9*, e1516. https://doi.org/10.7717/peerj-cs.1516

Alam, S., Gebremichael, M., Ban, Z., Scanlon, B. R., Senay, G., & Lettenmaier, D. P. (2021). Post-drought groundwater storage recovery in California's Central Valley. *Water Resources Research*, *57*(10), e2021WR030352. https://doi.org/10.1029/2021WR030352

Allen, E. B., Rittenour, T. M., DeRose, R. J., Bekker, M. F., Kjelgren, R., & Buckley, B. M. (2013). A tree-ring based reconstruction of Logan River streamflow, northern Utah. *Water Resources Research*, *49*(12), 8579–8588. https://doi.org/10.1002/2013WR014273

Baek, S. H., Smerdon, J. E., Coats, S., Williams, A. P., Cook, B. I., Cook, E. R., & Seager, R. (2017). Precipitation, temperature, and teleconnection signals across the combined North American, Monsoon Asia, and Old World Drought Atlases. *Journal of Climate*, *30*(18), 7141–7155. https://doi.org/10.1175/JCLI-D-16-0766.1

Baek, S. H., Smerdon, J. E., Seager, R., Williams, A. P., & Cook, B. I. (2019a). Pacific Ocean forcing and atmospheric variability are the dominant causes of spatially widespread droughts in the contiguous United States. *Journal of Geophysical Research: Atmospheres*, *124*(5), 2507–2524. https://doi.org/10.1029/2018JD029219

Baek, S. H., Steiger, N. J., Smerdon, J. E., & Seager, R. (2019b). Oceanic drivers of widespread summer droughts in the United States over the Common Era. *Geophysical Research Letters*, *46*(14), 8271–8280. https://doi.org/10.1029/2019GL082838

Benson, L., Petersen, K., & Stein, J. (2007). Anasazi (Pre-Columbian Native-American) migrations during the middle-12th and late-13th centuries–were they drought induced? *Climatic Change*, *83*(1), 187–213. https://doi.org/10.1007/s10584-006-9065-y

Bishop, D. A., Williams, A. P., Seager, R., Cook, E. R., Peteet, D. M., Cook, B. I., et al. (2021). Placing the east-west North American aridity gradient in a multi-century context. *Environmental Research Letters*, *16*(11), 114043. https://doi.org/10.1088/1748-9326/ac2f63

Christensen, N. S., Wood, A. W., Voisin, N., Lettenmaier, D. P., & Palmer, R. N. (2004). The effects of climate change on the hydrology and water resources of the Colorado River Basin. *Climatic Change*, *62*(1–3), 337–363. https://doi.org/10.1023/B:CLIM.0000013684.13621.1f

Coats, S., Smerdon, J. E., Cook, B. I., Seager, R., Cook, E. R., & Anchukaitis, K. J. (2016). Internal ocean-atmosphere variability drives megadroughts in Western North America. *Geophysical Research Letters*, *43*(18), 9886–9894. https://doi.org/10.1002/2016GL070105

Cook, B., & Marvel, K. D. (2024). bcook/pluvial: V1 [Software]. *Zenodo*. https://doi.org/10.5281/zenodo.13799310

Cook, B. I., Ault, T. R., & Smerdon, J. E. (2015). Unprecedented 21st century drought risk in the American southwest and Central Plains. *Science Advances*, *1*(1), e1400082. https://doi.org/10.1126/sciadv.1400082

Cook, B. I., Mankin, J. S., Marvel, K., Williams, A. P., Smerdon, J. E., & Anchukaitis, K. J. (2020). Twenty-first century drought projections in the CMIP6 forcing scenarios. *Earth's Future*, *8*(6), e2019EF001461. https://doi.org/10.1029/2019EF001461

Cook, B. I., Mankin, J. S., Williams, A. P., Marvel, K. D., Smerdon, J. E., & Liu, H. (2021). Uncertainties, limits, and benefits of climate change mitigation for soil moisture drought in Southwestern North America. *Earth's Future*, *9*(9), e2021EF002014. https://doi.org/10.1029/2021EF002014

Cook, B. I., Miller, R. L., & Seager, R. (2009). Amplification of the North American "Dust Bowl" drought through human-induced land degradation. *Proceedings of the National Academy of Sciences*, *106*(13), 4997–5001. https://doi.org/10.1073/pnas.0810200106

Cook, B. I., Seager, R., & Miller, R. L. (2011). On the causes and dynamics of the early twentieth-century North American pluvial. *Journal of Climate*, *24*(19), 5043–5060. https://doi.org/10.1175/2011JCLI4201.1

Cook, B. I., Smerdon, J. E., Cook, E. R., Williams, A. P., Anchukaitis, K. J., Mankin, J. S., et al. (2022). Megadroughts in the Common Era and the Anthropocene. *Nature Reviews Earth & Environment*, *3*(11), 741–757. https://doi.org/10.1038/s43017-022-00329-1

Cook, E. R., Seager, R., Heim Jr, R. R., Vose, R. S., Herweijer, C., & Woodhouse, C. (2010). Megadroughts in North America: Placing IPCC projections of hydroclimatic change in a long-term palaeoclimate context. *Journal of Quaternary Science*, *25*(1), 48–61. https://doi.org/10.1002/jqs.1303

Culver, L. (2012). The Desert and the Garden: Climate as attractor and obstacle in the settlement history of the western United States. *Global Environment*, *5*(9), 130–159. https://doi.org/10.3197/ge.2012.050906

Dennison, P. E., Brewer, S. C., Arnold, J. D., & Moritz, M. A. (2014). Large wildfire trends in the western United States, 1984–2011. *Geophysical Research Letters*, *41*(8), 2928–2933. https://doi.org/10.1002/2014GL059576

Fall, A., & Davis, A. (2022). *Problems of imperial valley and vicinity*. U.S. Gov. Print. Off. Retrieved from https://hdl.handle.net/2027/hvd.32044031907595

Fleck, J., & Castle, A. (2022). Green light for adaptive policies on the Colorado River. *Water*, *14*(1), 2. https://doi.org/10.3390/w14010002

Forsythe, K. W., Schatz, B., Swales, S. J., Ferrato, L.-J., & Atkinson, D. M. (2012). Visualization of lake Mead surface area changes from 1972 to 2009. *ISPRS International Journal of Geo-Information*, *1*(2), 108–119. https://doi.org/10.3390/ijgi1020108

Fritts, H. (1976). *Tree rings and climate*. Elsevier.

Fye, F. K., Stahle, D. W., & Cook, E. R. (2003). Paleoclimatic analogs to twentieth-century moisture regimes across the United States. *Bulletin of the American Meteorological Society*, *84*(7), 901–909. https://doi.org/10.1175/BAMS-84-7-901

Ge, S., Silverstein, J., Eklund, J., Limerick, P., & Stewart, D. (2023). Fixing the flawed Colorado River Compact. *Eos, Transactions of the American Geophysical Union*, *104*. https://doi.org/10.1029/2023EO230232

Gillies, S. (2007). Shapely: Manipulation and analysis of geometric objects [Software]. https://github.com/Toblerity/Shapely

Harris, C. R., Millman, K. J., van der Walt, S. J., Gommers, R., Virtanen, P., Cournapeau, D., et al. (2020). Array programming with NumPy [Software]. *Nature*, *585*(7825), 357–362. https://doi.org/10.1038/s41586-020-2649-2

Herweijer, C., Seager, R., & Cook, E. R. (2006). North American droughts of the mid to late nineteenth century: A history, simulation and implication for Mediaeval drought. *The Holocene*, *16*(2), 159–171. https://doi.org/10.1191/0959683606hl917rp

Herweijer, C., Seager, R., Cook, E. R., & Emile-Geay, J. (2007). North American droughts of the last millennium from a gridded network of tree-ring data. *Journal of Climate*, *20*(7), 1353–1376. https://doi.org/10.1175/JCLI4042.1

Holdren, G. C., & Turner, K. (2010). Characteristics of lake Mead, Arizona–Nevada. *Lake and Reservoir Management*, *26*(4), 230–239. https://doi.org/10.1080/07438141.2010.540699

Hua, W., Dai, A., & Qin, M. (2018). Contributions of internal variability and external forcing to the recent Pacific decadal variations. *Geophysical Research Letters*, *45*(14), 7084–7092. https://doi.org/10.1029/2018GL079033

Huang, B., Thorne, P. W., Banzon, V. F., Boyer, T., Chepurin, G., Lawrimore, J. H., et al. (2017). NOAA extended reconstructed sea surface temperature (ERSST), version 5. *NOAA National Centers for Environmental Information*.

Huang, H.-P., Seager, R., & Kushnir, Y. (2005). The 1976/77 transition in precipitation over the Americas and the influence of tropical sea surface temperature. *Climate Dynamics*, *24*(7), 721–740. https://doi.org/10.1007/s00382-005-0015-6

Hunter, J. D. (2007). Matplotlib: A 2D graphics environment [Software]. *Computing in Science & Engineering*, *9*(3), 90–95. https://doi.org/10.1109/MCSE.2007.55

Juang, C. S., Williams, A. P., Abatzoglou, J. T., Balch, J. K., Hurteau, M. D., & Moritz, M. A. (2022). Rapid growth of large forest fires drives the Exponential response of annual forest-fire area to aridity in the western United States. *Geophysical Research Letters*, *49*(5), e2021GL097131. https://doi.org/10.1029/2021GL097131

Kennedy, J. J., Rayner, N. A., Atkinson, C. P., & Killick, R. E. (2019). An ensemble data set of sea surface temperature change from 1850: The met Office Hadley Centre HadSST.4.0.0.0 data set. *Journal of Geophysical Research: Atmospheres*, *124*(14), 7719–7763. https://doi.org/10.1029/2018JD029867

Kuhn, E., & Fleck, J. (2019). *Science be dammed: How ignoring inconvenient science drained the Colorado River*. University of Arizona Press.

Kumar, R., Carroll, C., Hartikainen, A., & Martin, O. (2019). ArviZ a unified library for exploratory analysis of Bayesian models in Python [Software]. *Journal of Open Source Software*, *4*(33), 1143. https://doi.org/10.21105/joss.01143

Kushnir, Y., Seager, R., Ting, M., Naik, N., & Nakamura, J. (2010). Mechanisms of tropical Atlantic SST influence on North American precipitation variability. *Journal of Climate*, *23*(21), 5610–5628. https://doi.org/10.1175/2010JCLI3172.1

La Rue, E. C., Work, H., & Grover, N. C. (1925). Water power and flood control of Colorado River below Green River, Utah (Tech. Rep.). *U.S. Geological Survey Water Supply Paper 556*. https://doi.org/10.3133/wsp556

Mankin, J. S., Seager, R., Smerdon, J. E., Cook, B. I., & Williams, A. P. (2019). Mid-latitude freshwater availability reduced by projected vegetation responses to climate change. *Nature Geoscience*, *12*(12), 983–988. https://doi.org/10.1038/s41561-019-0480-x

Mann, M. E., Steinman, B. A., Brouillette, D. J., & Miller, S. K. (2021). Multidecadal climate oscillations during the past millennium driven by volcanic forcing. *Science*, *371*(6533), 1014–1019. https://doi.org/10.1126/science.abc5810

Mantua, N. J., Hare, S. R., Zhang, Y., Wallace, J. M., & Francis, R. C. (1997). A Pacific interdecadal climate oscillation with impacts on salmon production. *Bulletin of the American Meteorological Society*, *78*(6), 1069–1079. https://doi.org/10.1175/1520-0477(1997)078⟨1069:APICOW⟩2.0.CO;2

McCabe, G. J., Palecki, M. A., & Betancourt, J. L. (2004). Pacific and Atlantic Ocean influences on multidecadal drought frequency in the United States. *Proceedings of the National Academy of Sciences*, *101*(12), 4136–4141. https://doi.org/10.1073/pnas.0306738101

Meko, D. M., Woodhouse, C. A., Baisan, C. A., Knight, T., Lukas, J. J., Hughes, M. K., & Salzer, M. W. (2007). Medieval drought in the upper Colorado River Basin. *Geophysical Research Letters*, *34*(10), 10705–10709. https://doi.org/10.1029/2007GL029988

Meko, D. M., Woodhouse, C. A., & Winitsky, A. G. (2022). Tree-ring perspectives on the Colorado River: Looking back and moving forward. *JAWRA Journal of the American Water Resources Association*, *58*(5), 604–621. https://doi.org/10.1111/1752-1688.12989

Menard, A. (2011). Striking a line through the Great American Desert. *Journal of American Studies*, *45*(2), 267–280. https://doi.org/10.1017/S0021875810000034

Met Office. (2010-2015). Cartopy: A cartographic python library with a matplotlib interface [Software] [Computer Software Manual]. *Exeter, Devon*. Retrieved from https://scitools.org.uk/cartopy

Morris, R. C. (1926). The notion of a great American desert east of the rockies. *The Mississippi Valley Historical Review*, *13*(2), 190–200. https://doi.org/10.2307/1891956

Nemani, R., White, M., Thornton, P., Nishida, K., Reddy, S., Jenkins, J., & Running, S. (2002). Recent trends in hydrologic balance have enhanced the terrestrial carbon sink in the United States. *Geophysical Research Letters*, *29*(10), 106-1–106-4. https://doi.org/10.1029/2002GL014867

Newman, M., Alexander, M. A., Ault, T. R., Cobb, K. M., Deser, C., Di Lorenzo, E., et al. (2016). The pacific decadal oscillation, revisited. *Journal of Climate*, *29*(12), 4399–4427. https://doi.org/10.1175/JCLI-D-15-0508.1

Nielsen, M., Cook, B. I., Marvel, K., Ting, M., & Smerdon, J. E. (2024). The changing influence of precipitation on soil moisture drought with warming in the mediterranean and western North America. *Earth's Future*, *12*(5), e2023EF003987. https://doi.org/10.1029/2023EF003987

Nigam, S., Guan, B., & Ruiz-Barradas, A. (2011). Key role of the atlantic multidecadal oscillation in 20th century drought and wet periods over the Great Plains. *Geophysical Research Letters*, *38*(16), L16713. https://doi.org/10.1029/2011GL048650

Oglesby, R., Feng, S., Hu, Q., & Rowe, C. (2012). The role of the Atlantic Multidecadal Oscillation on medieval drought in North America: Synthesizing results from proxy data and climate models. *Global and Planetary Change*, *84–85*(0), 56–65. https://doi.org/10.1016/j.gloplacha.2011.07.005

pandas development team, T. (2020). pandas-dev/pandas: Pandas [Software]. *Zenodo*. https://doi.org/10.5281/zenodo.3509134

Pérez, F., & Granger, B. E. (2007). IPython: A system for interactive scientific computing [Software]. *Computing in Science & Engineering*, *9*(3), 21–29. https://doi.org/10.1109/MCSE.2007.53

Qin, M., Dai, A., & Hua, W. (2020). Quantifying contributions of internal variability and external forcing to Atlantic multidecadal variability since 1870. *Geophysical Research Letters*, *47*(22), e2020GL089504. https://doi.org/10.1029/2020GL089504

Rahmati, M., Amelung, W., Brogi, C., Dari, J., Flammini, A., Bogena, H., et al. (2024). Soil moisture memory: State-Of-The-Art and the way forward. *Reviews of Geophysics*, *62*(2), e2023RG000828. https://doi.org/10.1029/2023RG000828

Rasker, R. (2016). West's economy outperforming rest of United States (Tech. Rep.). *Headwaters Economics*.

Rayner, N. A., Parker, D. E., Horton, E. B., Folland, C. K., Alexander, L. V., Rowell, D. P., et al. (2003). Global analyses of sea surface temperature, sea ice, and night marine air temperature since the late nineteenth century. *Journal of Geophysical Research*, *108*(D14), 4407. https://doi.org/10.1029/2002JD002670

Robeson, S. M., Maxwell, J. T., & Ficklin, D. L. (2020). Bias correction of paleoclimatic reconstructions: A new look at 1,200+ years of upper Colorado River flow. *Geophysical Research Letters*, *47*(1), e2019GL086689. https://doi.org/10.1029/2019GL086689

Schubert, S., Gutzler, D., Wang, H., Dai, A., Delworth, T., Deser, C., et al. (2009). A US CLIVAR Project to assess and compare the responses of global climate models to drought-related SST forcing patterns: Overview and results. *Journal of Climate*, *22*(19), 5251–5272. https://doi.org/10.1175/2009JCLI3060.1

Schubert, S. D., Chang, Y., DeAngelis, A. M., Lim, Y.-K., Thomas, N. P., Koster, R. D., et al. (2024). Insights into the causes and predictability of the 2022/23 California flooding. *Journal of Climate*, *37*(13), 3613–3629. https://doi.org/10.1175/JCLI-D-23-0696.1

Schubert, S. D., Suarez, M. J., Pegion, P. J., Koster, R. D., & Bacmeister, J. T. (2004). On the cause of the 1930s Dust Bowl. *Science*, *303*(5665), 1855–1859. https://doi.org/10.1126/science.1095048

Seabold, S., & Perktold, J. (2010). statsmodels: Econometric and statistical modeling with python [Software]. In *9th python in science conference*. https://doi.org/10.25080/Majora-92bf1922-011

Seager, R., Kushnir, Y., Herweijer, C., Naik, N., & Velez, J. (2005). Modeling of tropical forcing of persistent droughts and pluvials over western North America: 1856–2000. *Journal of Climate*, *18*(19), 4065–4088. https://doi.org/10.1175/JCLI3522.1

Seager, R., & Ting, M. (2017). Decadal drought variability over North America: Mechanisms and predictability. *Current Climate Change Reports*, *3*(2), 141–149. https://doi.org/10.1007/s40641-017-0062-1

Seager, R., Ting, M., Alexander, P., Liu, H., Nakamura, J., Li, C., & Newman, M. (2023). Ocean-forcing of cool season precipitation drives ongoing and future decadal drought in Southwestern North America. *npj Climate and Atmospheric Science*, *6*(1), 141. https://doi.org/10.1038/s41612-023-00461-9

Slivinski, L. C., Compo, G. P., Sardeshmukh, P. D., Whitaker, J. S., McColl, C., Allan, R. J., et al. (2021). An evaluation of the performance of the twentieth century reanalysis version 3. *Journal of Climate*, *34*(4), 1417–1438. https://doi.org/10.1175/JCLI-D-20-0505.1

Steiger, N. J. (2018). Paleo hydrodynamics data assimilation product (phyda) [Dataset]. *Zenodo*. https://doi.org/10.5281/zenodo.1198817

Steiger, N. J., Smerdon, J. E., Cook, B. I., Seager, R., Williams, A. P., & Cook, E. R. (2019). Oceanic and radiative forcing of medieval megadroughts in the American Southwest. *Science Advances*, *5*(7), eaax0087. https://doi.org/10.1126/sciadv.aax0087

Steiger, N. J., Smerdon, J. E., Cook, E. R., & Cook, B. I. (2018). A reconstruction of global hydroclimate and dynamical variables over the Common Era. *Scientific Data*, *5*(1), 180086. https://doi.org/10.1038/sdata.2018.86

Steiger, N. J., Smerdon, J. E., Seager, R., Williams, A. P., & Varuolo-Clarke, A. M. (2021). ENSO-driven coupled megadroughts in North and South America over the last millennium. *Nature Geoscience*, *14*(10), 739–744. https://doi.org/10.1038/s41561-021-00819-9

St. George, S., Meko, D., & Cook, E. (2010). The seasonality of precipitation signals embedded within the North American Drought Atlas. *The Holocene*, *20*(6), 983–988. https://doi.org/10.1177/0959683610365937

Stockton, C. W., & Jacoby, G. C. J. (1976). Long-term surface-water supply and streamflow trends in the upper Colorado River Basin. *Lake Powell Research Project Bulletin*, *1*(18).

Sun, Y., Bekker, M. F., DeRose, R. J., Kjelgren, R., & Wang, S. Y. S. (2017). Statistical treatment for the wet bias in tree-ring chronologies: A case study from the interior west, USA. *Environmental and Ecological Statistics*, *24*(1), 131–150. https://doi.org/10.1007/s10651-016-0363-x

Team, T. M. D. (2024). Matplotlib: Visualization with Python [Software]. *Zenodo*. https://doi.org/10.5281/ZENODO.13308876

Tejedor, E., Steiger, N. J., Smerdon, J. E., Serrano-Notivoli, R., & Vuille, M. (2021). Global hydroclimatic response to tropical volcanic eruptions over the last millennium. *Proceedings of the National Academy of Sciences*, *118*(12), e2019145118. https://doi.org/10.1073/pnas.2019145118

Thirumalai, K., Quinn, T. M., Okumura, Y., Richey, J. N., Partin, J. W., Poore, R. Z., & Moreno-Chamarro, E. (2018). Pronounced centennial-scale Atlantic Ocean climate variability correlated with Western Hemisphere hydroclimate. *Nature Communications*, *9*(1), 392. https://doi.org/10.1038/s41467-018-02846-4

Ting, M., Kushnir, Y., Seager, R., & Li, C. (2011). Robust features of Atlantic multi-decadal variability and its climate impacts. *Geophysical Research Letters*, *38*(17), L17705. https://doi.org/10.1029/2011GL048712

Triacca, U., & Pasini, A. (2024). On the unforced or forced nature of the Atlantic multidecadal oscillation: A linear and nonlinear causality analysis. *Climate*, *12*(7), 90. https://doi.org/10.3390/cli12070090

van der Schrier, G., & Barkmeijer, J. (2007). North American 1818–1824 drought and 1825–1840 pluvial and their possible relation to the atmospheric circulation. *Journal of Geophysical Research*, *112*(D13), D13102. https://doi.org/10.1029/2007JD008429

Van Rossum, G., & Drake, F. L. (2009). Python 3 reference manual [Software]. *CreateSpace*. https://doi.org/10.5555/1593511

Virtanen, P., Gommers, R., Oliphant, T. E., Haberland, M., Reddy, T., Cournapeau, D., et al. (2020). SciPy 1.0: Fundamental algorithms for scientific computing in Python [Software]. *Nature Methods*, *17*(3), 261–272. https://doi.org/10.1038/s41592-019-0686-2

Vose, R. S., Applequist, S., Squires, M., Durre, I., Menne, M., Williams, C., et al. (2014). NOAA monthly US Climate gridded dataset (NClimGrid), Version 1 subset over Southwestern North America [Dataset]. *NOAA National Centers for Environmental Information*. https://doi.org/10.7289/V5SX6B56

Waskom, M. L. (2021). seaborn: Statistical data visualization [Software]. *Journal of Open Source Software*, *6*(60), 3021. https://doi.org/10.21105/joss.03021

Wes McKinney. (2010). Data structures for statistical computing in Python [Software]. *Proceedings of the 9th Python in science conference*. In S. van der Walt, & J. Millman (Eds.) (pp. 56–61). https://doi.org/10.25080/Majora-92bf1922-00a

Williams, A. P. (2024). Soil moisture reconstruction [Dataset]. *Zenodo*. https://doi.org/10.5281/zenodo.13755272

Williams, A. P., Cook, B. I., & Smerdon, J. E. (2022). Rapid intensification of the emerging Southwestern North American megadrought in 2020–2021. *Nature Climate Change*, *12*(3), 232–234. https://doi.org/10.1038/s41558-022-01290-z

Williams, A. P., Cook, E. R., Smerdon, J. E., Cook, B. I., Abatzoglou, J. T., Bolles, K., et al. (2020). Large contribution from anthropogenic warming to an emerging North American megadrought. *Science*, *368*(6488), 314–318. https://doi.org/10.1126/science.aaz9600

Woodhouse, C. A., Gray, S. T., & Meko, D. M. (2006). Updated streamflow reconstructions for the upper Colorado River Basin. *Water Resources Research*, *42*(5). https://doi.org/10.1029/2005WR004455

Woodhouse, C. A., Kunkel, K. E., Easterling, D. R., & Cook, E. R. (2005). The twentieth-century pluvial in the western United States. *Geophysical Research Letters*, *32*(7), L07701. https://doi.org/10.1029/2005GL022413

Woodhouse, C. A., Meko, D. M., & Bigio, E. R. (2020). A long view of southern California water supply: Perfect droughts revisited. *JAWRA Journal of the American Water Resources Association*, *56*(2), 212–229. https://doi.org/10.1111/1752-1688.12822